Journal of Applied Polymer Science

PLA/Sepiolite and PLA/Calcium Carbonate Nanocomposites: A Comparison Study

Mohammad Sabzi,[1,2] Long Jiang,[2] Mohammad Atai,[1] Ismail Ghasemi[1]

[1]Iran Polymer and Petrochemical Institute (IPPI), 14965/115, Tehran, Iran

[2]Department of Mechanical Engineering, North Dakota State University, Fargo, North Dakota 58108

Correspondence to: L. Jiang (E-mail: long.jiang@ndsu.edu) or M. Atai (E-mail: m.atai@ippi.ac.ir)

ABSTRACT: Polylactic acid (PLA)-based nanocomposites comprising two different types of nanofillers, i.e. sepiolite (SEP) and nano calcium carbonate (NCC), were prepared by internal mixing and injection molding. Because of the different aspect ratio, surface area, and surface property of the nanofillers, their effects on the morphological, mechanical, dynamic mechanical, rheological, and thermal properties of the nanocomposites were shown to be very different. NCC demonstrated more uniform particle dispersion and matrix compatibility than did SEP because of the former's surface treatment, thus leading to higher strength and strain-at-failure of PLA/NCC composites. On the other hand, larger aspect ratio and surface area of SEP caused higher melt viscosity, stronger shear thinning, and better thermal resistance of PLA/SEP composites. © 2012 Wiley Periodicals, Inc. J. Appl. Polym. Sci. 129: 1734–1744, 2013

KEYWORDS: clay; biopolymers and renewable polymers; composites; mechanical properties; nanoparticles; nanowires and nanocrystals

Received 29 August 2011; accepted 19 November 2012; published online 19 December 2012

DOI: 10.1002/app.38866

INTRODUCTION

Biodegradable and bio-based polymers have attracted much attention because of the environmental concerns and sustainability issues associated with petroleum-based polymers. Among the commercialized bio-based polymers, PLA has the largest volume of production and has been used in various end-use applications. PLA has many advantages such as biocompatibility, high strength and modulus, outstanding processability, and low carbon footprint.[1] However, the toughness, heat deflection temperature, flexural and gas barrier properties of PLA are inferior to those of commodity polymers such as polypropylene. These properties can be improved by adding nanoparticles to the polymer. Various nano-reinforcements including layered-silicate clays,[2–6] silica,[7,8] cellulose nanofibers,[9–12] nanoTiO_2,[13] nanodiamond,[14] nanotube,[15,16] nanographite,[4,17] and nano calcium carbonate[18,19] have been used with the aim of improving thermal, crystallization, mechanical, biodegradability, and melt rheological behaviors of polymers.

Most of the studies on clay nanocomposites have focused on layered silicates such as montmorillonite. Sepiolite, on the other hand, is a hydrated magnesium silicate ($Mg_4Si_6O_{15}(OH)_2{\cdot}6H_2O$) without layered structures. Its fibrous structure can be described as a quincunx of talc-type layers separated by parallel channels, which lead to relatively high surface area of sepiolite. Compared to layered silicates, the dispersion of sepiolite in polymer matrixes is easier due to its smaller surface area (with similar aspect ratio) and the resultant lower tendency toward agglomeration. Sepiolite has been shown to not only improve mechanical properties of polymer matrices[20–24] but also affected their rheological properties[25,26] and thermal stability.[27–33] PLA as the polymer matrix was used in four of these studies and the mechanical properties, biodegradability, crystallization, and thermal stability of the composites were investigated.[21,27,28,30] Rheological properties of PLA/sepiolite composites have not been studied and more in-depth mechanical property studies are also needed.

Nano calcium carbonate (nano-$CaCO_3$) particles have an aspect ratio of nearly 1. Its low production cost has led to its large scale applications in plastics, paints, inks industries, etc. It could noticeably improve both the toughness and stiffness of poly(vinyl chloride) (PVC), whereas showing small effect on the tensile strength.[34,35] It was also shown to be effective in improving the toughness of PLA.[18,36]

In this article, PLA/sepiolite and PLA/nano-$CaCO_3$ nanocomposites were prepared by internal mixing and injection molding. Morphological, mechanical, rheological, and thermal properties of the two composites were studied and compared. The effects of filler shape, surface area, and surface properties on the properties of the composites were discussed.

Table I. Formulations and Notations of the Nanocomposite Samples

Filler	Filler wt %	Filler vol %	Designation
	1	0.44	PLA/SEP1
Sepiolite (SEP)	3	1.34	PLA/SEP3
	5	2.25	PLA/SEP5
	10	4.64	PLA/SEP10
	1	0.47	PLA/NCC1
Nano-$CaCO_3$ (NCC)	3	1.43	PLA/NCC3
	5	2.40	PLA/NCC5
	10	4.94	PLA/NCC10

EXPERIMENTAL

Materials

PLA (3251D) was supplied by NatureWorks. Sepiolite (SEP) fibers with specific gravity of 2.83 g/cm^3 were supplied by Eskisehir (Turkey). The specific surface area of sepiolite (313.6 m^2/g) was measured through a nitrogen adsorption method (BET) using a surface area analyzer (Micrometrics Gremini III 2375). The nano-sized precipitated calcium carbonate (NCC, HAKUENKA® CC-RS) with an average particle size of 80 nm and specific gravity of 2.6–2.7g/cm^3 was supplied by Omya GmbH (Austria). A specific surface area of 17 m^2/g (by BET) was reported by the producer.[37] The powder was coated with fatty acids to improve its dispersion in organic matrixes.

Sample Preparation

Before use, PLA was dried at 80°C for 6 h and sepiolite and NCC powders were dried at 90°C for 12 h under vacuum. PLA/SEP and PLA/NCC composites (Table I) were prepared by mixing the materials in an internal mixer (Brabender, Germany) for 7 min (60 rpm, 180°C). Neat PLA was also processed using the same condition to prepare control samples. A mini injection molder (Dynisco Polymer Test, USA) was used to prepare tensile and DMA specimens. The melt and mold temperatures were set at 185 and 90°C, respectively.

Characterizations

Tensile properties of the nanocomposites were tested according to ASTM D638. The experiments were carried out on a universal testing machine (SMT-20, Santam, Iran) equipped with a 5 KN load cell. Tensile speed was 5 mm/min with a preload of 10 N. Test temperature was 23 ± 2°C. Young's modulus was calculated from the initial linear region of the stress–strain curves. Seven repeats were carried out for each sample.

Tescan (VEGAII, XMU, Czech Republic) Scanning Electron Microscopy (SEM) and HITACHI (S-4160, Japan) Field Emission Electron Microscopy (FESEM) were used to examine the morphology of the fracture surfaces obtained from the tensile test. The samples were sputter coated with gold before examination.

Dynamic mechanical properties of PLA and nanocomposites were evaluated using a dynamic mechanical analyzer (DMA) (Q 800, TA Instruments). DMA specimens (12.6 × 3.55 × 50 mm^3) were prepared by the mini injection molder and tested by a dual-cantilever fixture at a frequency of 1 Hz. All tests were carried out at a strain of 0.04% (within the linear region of the materials) with a 3°C/min temperature ramp from 30 to 120°C.

Rheological measurements were performed on a stress-controlled rheometer (AR G2, TA Instruments). Samples were tested at 180°C using a parallel-plate geometry (d = 25 mm). The distance between the plates was adjusted 1 mm. Initially, strain sweep test was performed to measure the linear viscoelastic limit of the PLA and nano composites. Dynamic frequency sweep measurements (strain: 5%, frequency: 0.05 to 600 rad/s) were conducted to evaluate the dynamic properties. Steady-shear tests were also conducted for all the samples at the same temperature (shear stress 0.005 to 7000 Pa).

Thermo gravimetric analysis (TGA) was carried out using a TGA-PL-150 (Polymer Laboratories) under nitrogen atmosphere (10°C/min, 25 to 700°C, sample size about 10 mg). Thermal degradation temperature was defined as the temperature at which 5% of weight loss ($T_{5\%}$) was obtained. T_{max} denotes the temperature at which the maximum weight loss rate occurred.

Differential scanning calorimetry (DSC) was performed using a DSC200F3 (Netzsch Instruments, Germany) under nitrogen atmosphere. All the samples were kept isothermally at 240°C for 3 min to erase their previous thermal history. They were then scanned from 240°C to 25°C at 10°C/min and subsequently from 25 to 240°C at 10°C/min.

The glass transition temperature (T_g), cold crystallization temperature (T_{cc}), melting temperature (T_m), cold crystallization enthalpy ($\triangle H_{cc}$), and melting enthalpy ($\triangle H_m$) were measured from the cooling and second heating scans. Crystallinity (χ) of PLA and the nanocomposites was calculated using the following equation:

$$\chi = \left(\frac{H_m}{H_m^0 \times (1 - m_f)}\right) \times 100\% \quad (1)$$

where $\triangle H_m$ is the specific melting enthalpy of the sample determined from the heating curves, $\triangle H_m^0$ is the melting enthalpy of the 100% crystalline PLA (93.0 J/g[4]) and m_f is the weight percentage of the fillers.[4]

RESULTS AND DISCUSSION

Morphology Studies

Determination of the Aspect Ratio of Nanoparticles. The sepiolite fibers used in this study demonstrated nonuniform length and diameter [Figure 1(a)]. Several white particles were believed to be dolomite impurities. The diameter and length of 270 fibers were measured using Image J software, and the data were analyzed using IBM SPSS statistics software to compute mean fiber length and diameter. The histograms of the fiber length and diameter are shown in Figure 2. The mean length and diameter of the fibers were calculated to be 7 μm and 340 nm, respectively, which resulted in a mean fiber aspect ratio (α) of 21. On the other hand, the aspect ratio of the NCC particles was close to one and the particle size was 80 nm [Figure 1(b)].

Tensile Fracture Surface. The tensile fracture surfaces of neat PLA and the two nanocomposites were examined by SEM

Applied Polymer SCIENCE

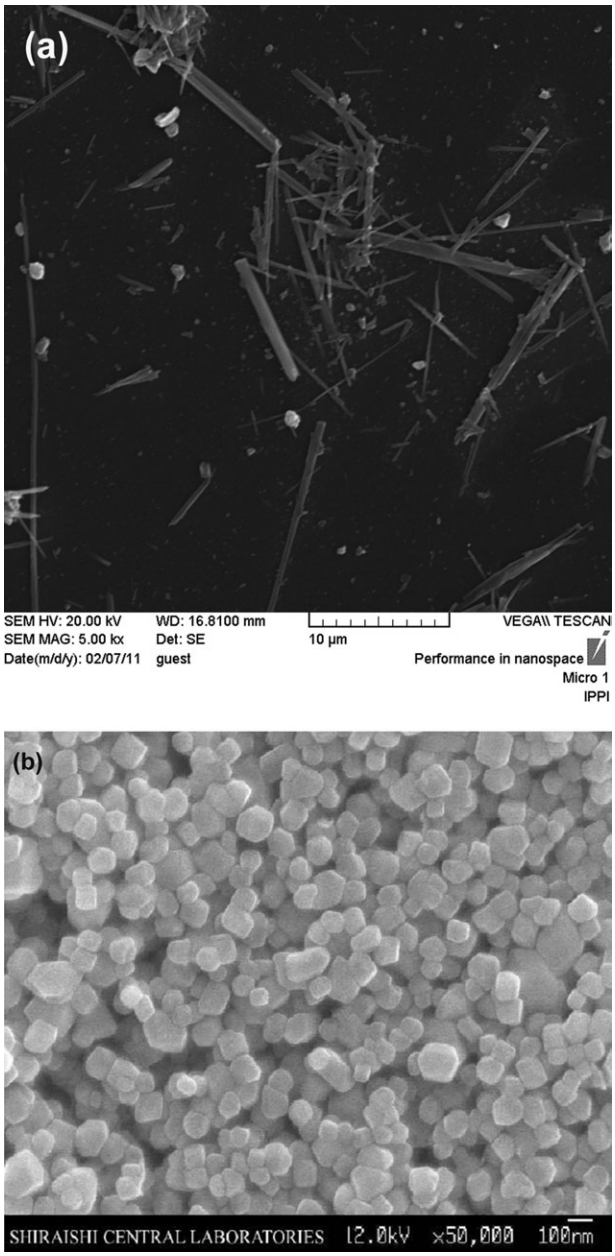

Figure 1. SEM images of sepiolite fibers (a) and nano calcium carbonate[1] (b).

(Figure 3). The composites containing SEP and NCC particles exhibited rougher and more irregular surfaces than that without fillers. Interfacial debonding at the filler–polymer interfaces initiated numerous cracks throughout the samples. Many of these cracks propagated through the samples and cause their ultimate fracture. The multiple crack propagation and diversion created the rough fracture surfaces of the nanocomposites. Without interfacial debonding, neat PLA showed a much smoother fracture surface. Figure 3 also shows that the nanoparticles tended to agglomerate at high particle concentrations and the sepiolite fibers appeared to be more prone to particle agglomeration compared to NCC at the same particle concentrations.

Under high magnification, individual SEP fibers and NCC particles can be seen on the fracture surfaces (Figure 4). SEP fibers showed interfacial debonding from the fracture surface, whereas NCC particles appeared to exhibit strong adhesion to the matrix polymer. The better dispersion of NCC and its stronger interfacial bonding with the PLA matrix was due to its fatty acid coating. On the other hand, without any surface treatment, SEP showed weaker interfacial bonding and the particles were more prone to particle agglomeration.

Tensile Properties

Tensile strength for the PLA/SEP and PLA/NCC composites are compared in Figure 5. Within the investigated particle concentration range, the strengths of all the composites were higher than that of the neat PLA. Both composites showed their maximum strengths at 1.4 vol % (3 wt %) particle concentration. The lower strengths at higher concentrations were most likely due to deteriorated particle dispersion. The strengths of the composites with 3 wt % SEP and NCC were 1.2 and 1.7 times

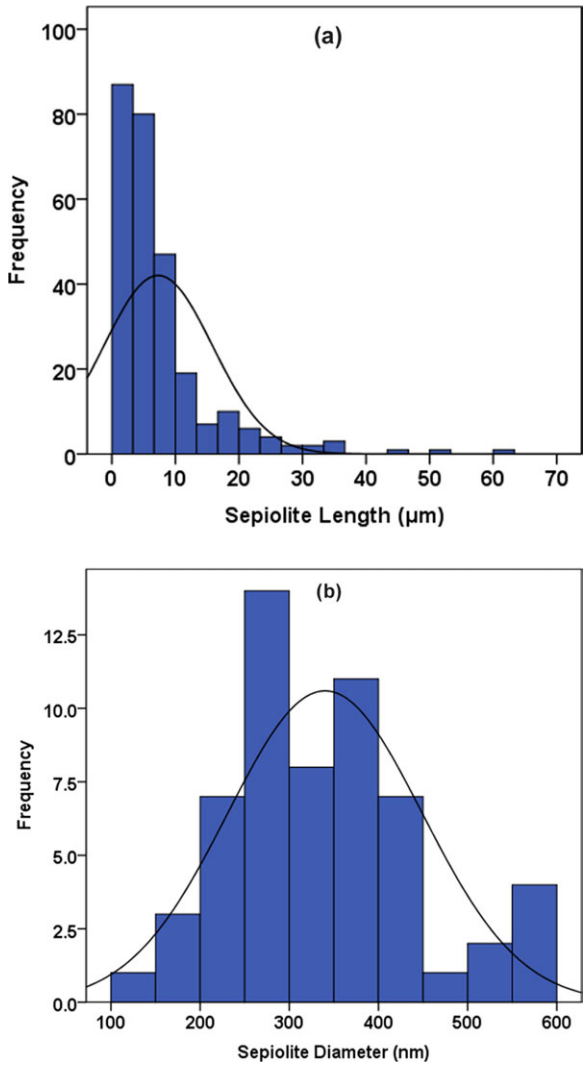

Figure 2. Histograms of sepiolite fiber length (a) and diameter (b). [Color figure can be viewed in the online issue, which is available at wileyonlinelibrary.com.]

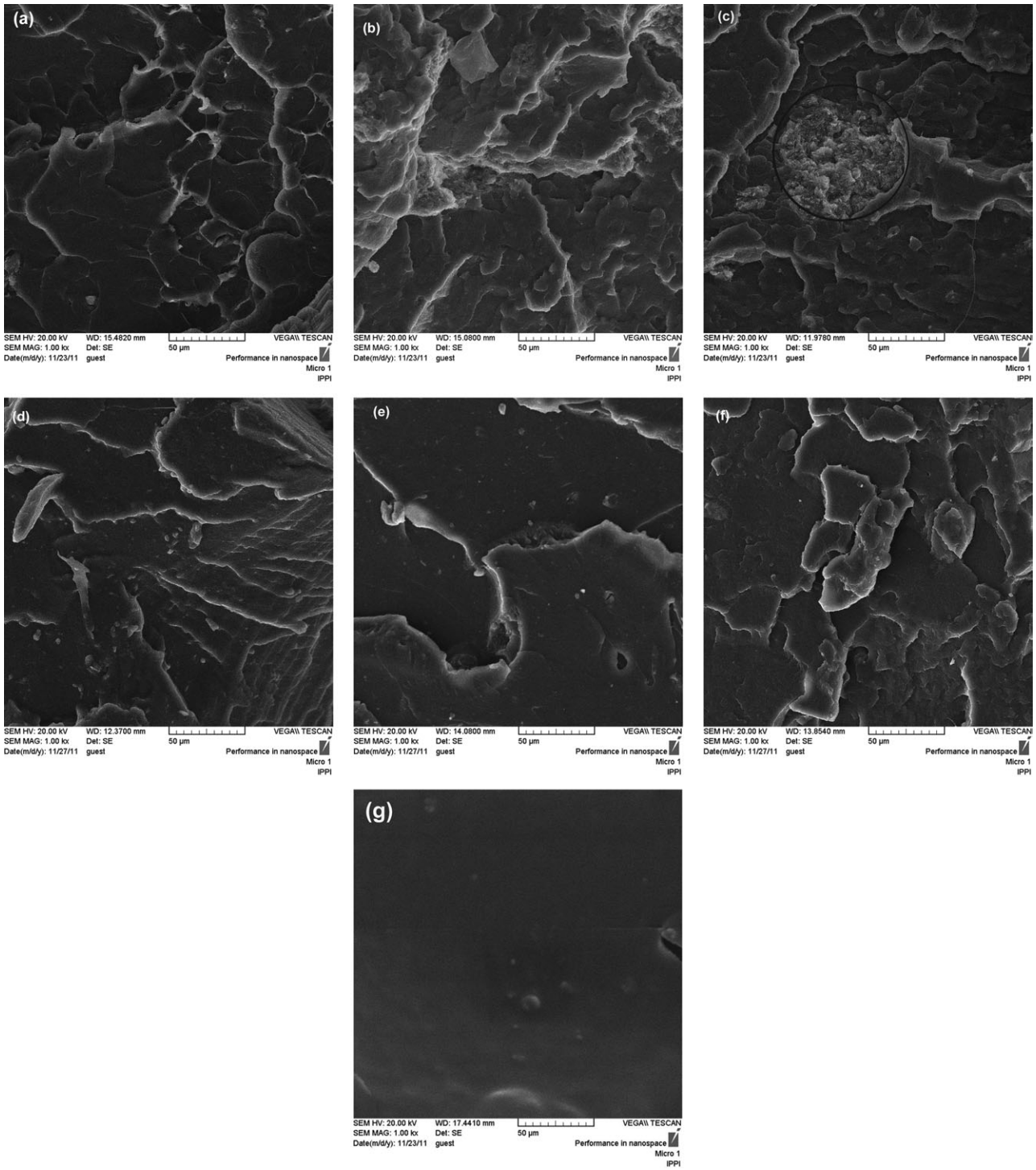

Figure 3. SEM images of the fracture surfaces after tensile test: 1 wt % SEP (a), 5 wt % SEP (b), 10 wt % SEP (c), 1 wt % NCC (d), 5 wt % NCC (e), 10 wt % NCC (f), nanocomposites and neat PLA (g) (the circle in the picture indicates SEP agglomerates).

of the strength of the neat PLA. Although SEP had larger aspect ratio than NCC (larger aspect ratio leads to higher reinforcement), the PLA/SEP composites exhibited significantly lower strength compared to the PLA/NCC composites at the same nanofiller loadings. This was believed to be due to NCCs stronger interfacial bonding and more homogeneous dispersion. With strong interfacial bonding, large stress can be transferred from the polymer matrix to the nano fillers, leading to high tensile strength.[35] The homogeneous dispersion of NCC also lowered the probability of forming large particle aggregates, which often causes stress concentrations and leads to premature sample failure. The strain-at-failure of the nanocomposites followed a trend similar to the tensile strength, i.e., the strain increased and then decreased as the nanoparticle content

Applied Polymer SCIENCE

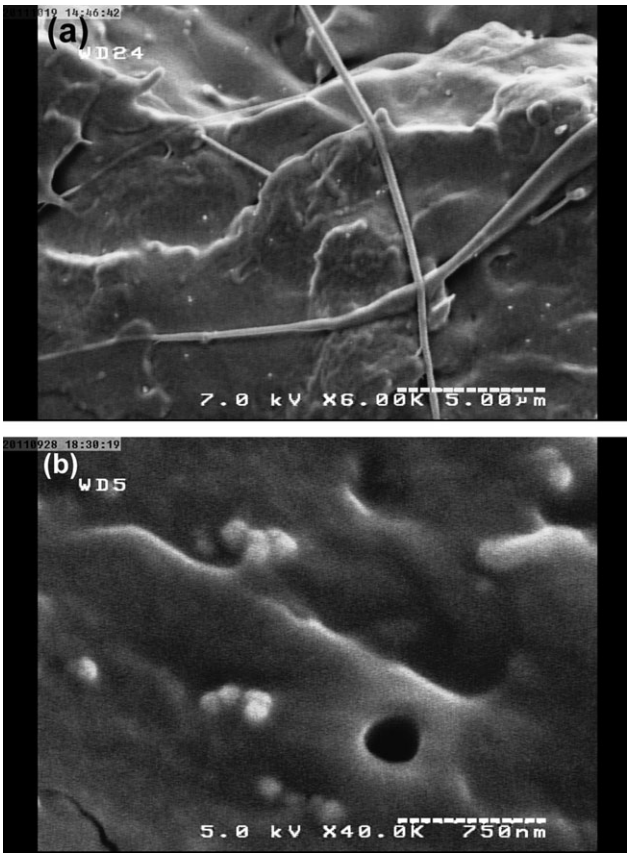

Figure 4. FESEM micrographs of the fracture surfaces of the PLA/SEP5 (a) and PLA/NCC5 (b) nanocomposites.

increased (Figure 6). This was because micro-sized agglomerates which appeared at high nanoparticle concentrations caused premature sample failures at low strains.

Tensile moduli of the neat PLA and the composites are presented in Figure 7. The moduli increased with increasing NCC and SEP contents within the entire filler content range. The

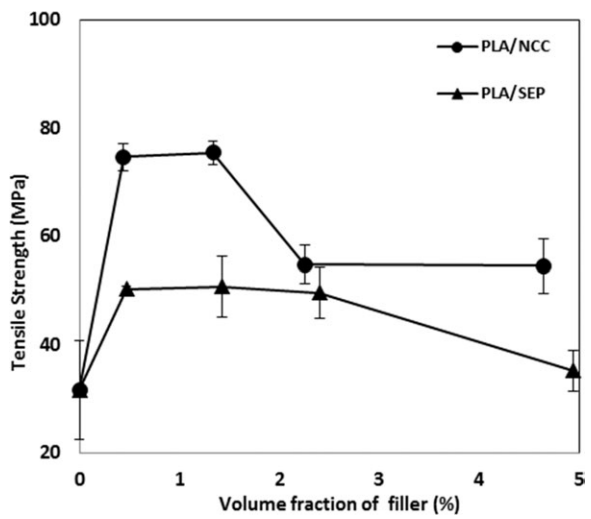

Figure 5. Tensile strength of PLA/SEP and PLA/NCC nanocomposites.

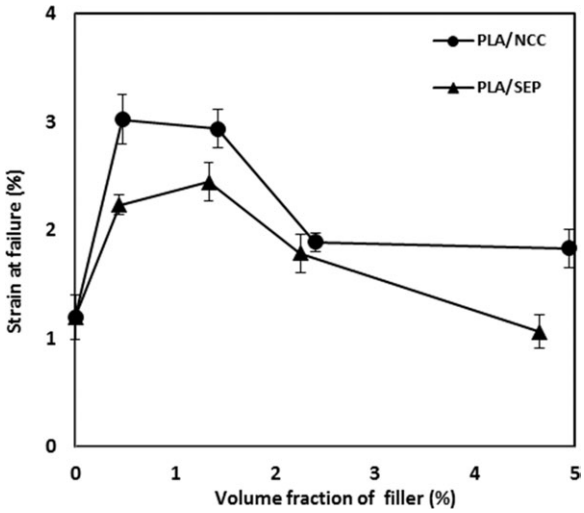

Figure 6. Strain at failure (%) of PLA/SEP and PLA/NCC nanocomposites at different filler loadings.

incorporation of 10 wt % of SEP and NCC (corresponding vol %: 4.64 and 4.94) led to a 25% and 19% increase in modulus, respectively. Halpin-Tsai micromechanical model was used to theoretically explain the trend of the moduli. The modulus for a composite (E_C) with randomly oriented short fibers is given as follows[38]:

$$Ec = \frac{3}{8}E_L + \frac{5}{8}E_T \tag{2}$$

where E_L and E_T are the longitudinal and transverse moduli of the composite, respectively. They can be calculated using the following equations:

$$\frac{E_L}{E_m} = \frac{1+\zeta\eta_L\varphi_r}{1-\eta_L\varphi_r} \quad \text{and} \quad \frac{E_T}{E_m} = \frac{1+2\eta_T\varphi_r}{1-\eta_T\varphi_r}$$
$$\eta_L = \frac{\frac{E_r}{E_m}-1}{\frac{E_r}{E_m}+\zeta} \quad \text{and} \quad \eta_T = \frac{\frac{E_r}{E_m}-1}{\frac{E_r}{E_m}+2} \tag{3}$$

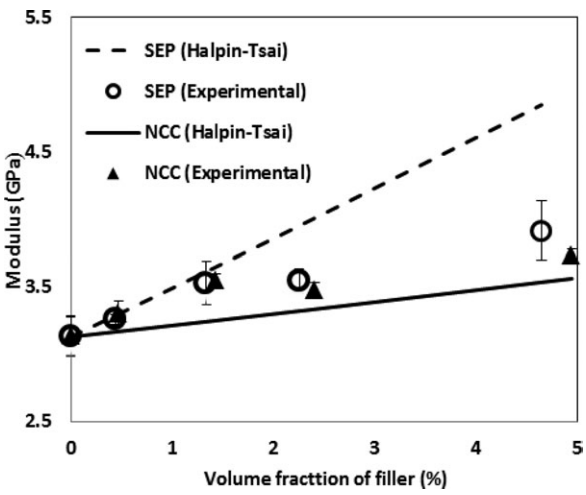

Figure 7. Comparison between experimental and theoretical values of the tensile moduli of PLA/SEP and PLA/NCC nanocomposites.

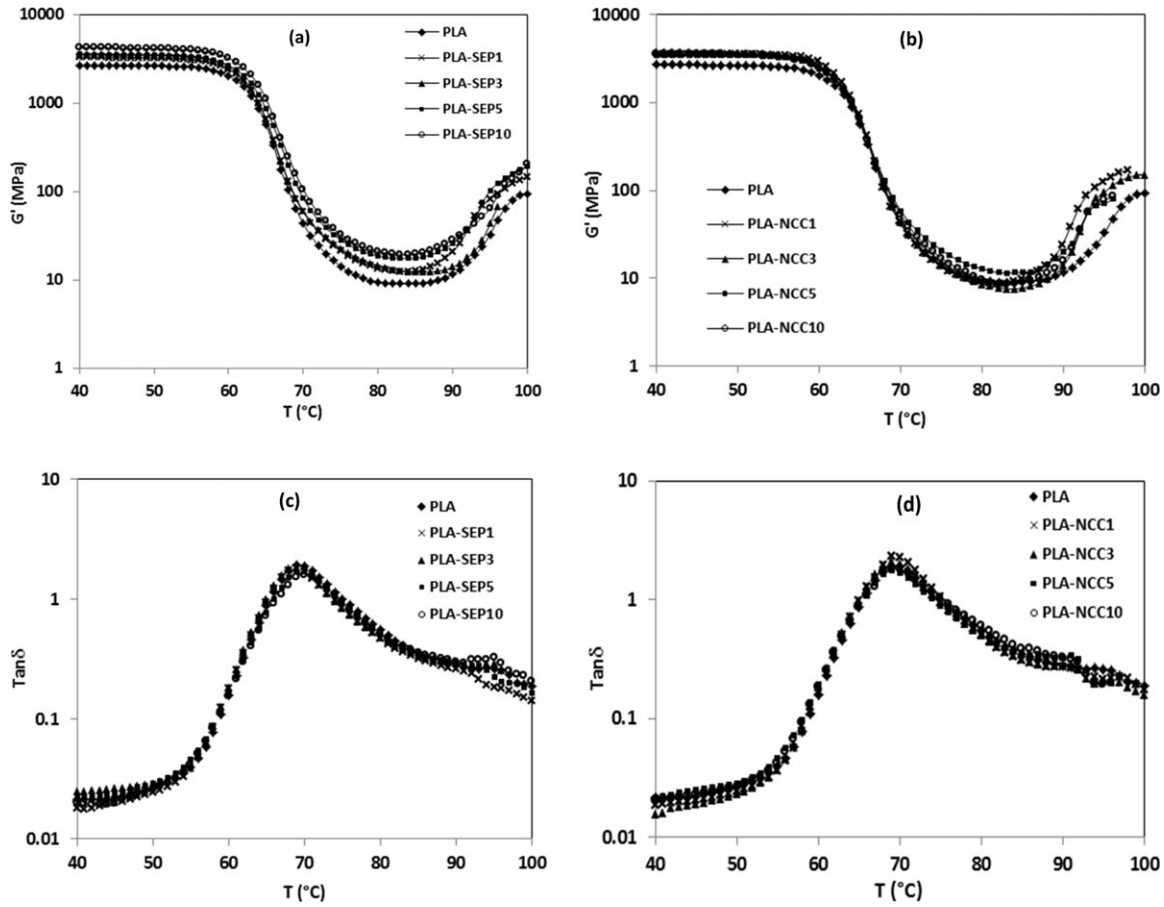

Figure 8. Storage modulus of PLA/SEP (a) and PLA/NCC (b) nanocomposites as a function of temperature and the corresponding tan δ curves (c) and (d).

where E_m is Young's modulus of the matrix and ζ is a shape factor which depends on the geometry and aspect ratio of the filler:

$$\zeta = (2L)/D \tag{4}$$

where L and D are the length and diameter of the filler, respectively. The L and D for sepiolite fibers were measured (from SEM micrographs) to be 7000 nm and 340 nm, respectively. The L/D of NCC particles was assumed to be 1 (diameter is about 80 nm). The volume fraction of the filler (φ_r) was calculated using the following equation:

$$\varphi_r = ((W_r/\rho_r)/((W_r/\rho_r) + (1 - W_r)/\rho_m) \tag{5}$$

where W_r and ρ_r are the weight percentage and density of the filler, respectively. ρ_m is the density of the matrix. The following values were used for model prediction: $\rho_m = 1.24$ g/cm^3, $E_m = 3.13$ GPa, $E_{SEP} = 200$ GPa,[20] $E_{NCC} = 26$ GPa,[39] $\rho_{SEP} = 2.2$ g/cm^3,[20] $\rho_{NCC} = 2.65$ g/cm^3.[40] Figure 7 compares the results of model prediction and experimental values. The figure shows that the experimental data of PLA/SEP composite agree well with its model prediction up to 1.4 vol % (3 wt %) and then deviate from the prediction by showing lower values. Wang et al. observed similar deviation in cellulose/biopolymer composites above 6 wt % filler concentration.[10] The deviation can be ascribed to SEP particle aggregation at high particle contents due to the low compatibility between PLA and SEP. By contrast, the experimental values of PLA/NCC composites were higher than the corresponding model predictions, as a result of good compatibility between PLA and the surface-coated NCC.[9]

Figure 7 shows that the predicted moduli of PLA/SEP composites are much higher than those of PLA/NCC because of SEPs higher aspect ratio. This model prediction is based on the assumption of perfect interfacial bonding and uniform particle dispersion. The fact that the two nanocomposites showed

Table II. Storage Modulus of PLA and Its Nanocomposites at the Temperatures Below and Above T_g

Sample	G' at 40°C (MPa)	G' at 80°C (MPa)	T_g (°C)
PLA	2702	9.4	69.2
PLA/SEP1	3315	9.2	68.8
PLA/SEP3	3625	13.7	68.5
PLA/SEP5	3582	18.8	69.4
PLA/SEP10	4274	21.1	69.8
PLA/NCC1	3564	9.2	69.3
PLA/NCC3	3591	8.9	69.1
PLA/NCC5	3761	12.8	68.9
PLA/NCC10	3480	9.4	69.1

Applied Polymer SCIENCE

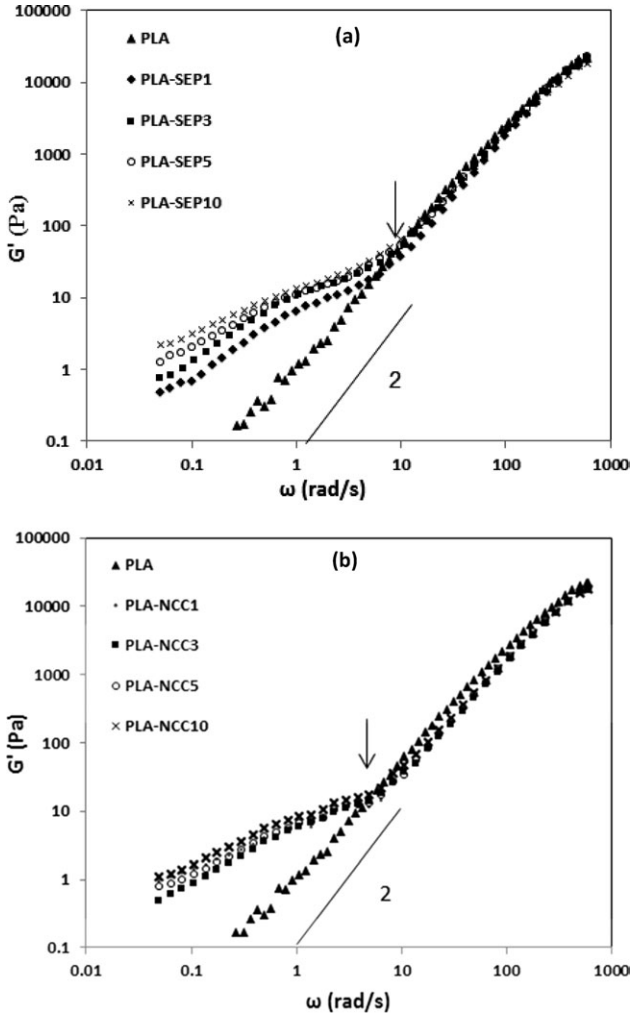

Figure 9. Storage modulus of PLA/SEP (a) and PLA/NCC (b) nanocomposites as a function of angular speed.

similar experimental moduli indicates that NCC exhibited better dispersion and stronger interfacial bonding than SEP did.

A percolation theory has been used to explain abrupt property increase in fiber-reinforced composites.[41] When percolation occurs, dispersed particles transition from a disconnected set of objects to an infinitely connected state and the properties of the composite often exhibit abrupt changes. The geometrical percolation threshold φ_c (volume fraction) of the particles can be calculated using the equation given below[42]:

$$\varphi_c = 1 - e^{-(cv/v_{ex})} \quad (6)$$

where v is the volume of the particle, v_{ex} is the excluded volume of the particle, c is the total excluded volume in an infinite system. For randomly oriented cylindrical particles (e.g., the sepiolite fibers in this study), the equation can be further developed into[42]:

$$\phi_c = 1 - \exp\left(-\frac{c\left(\left(\frac{4}{3}\right)\pi r^3 + \pi r^2 L\right)}{\frac{4}{3}\pi(2r)^3 + 2\pi(2r)^2 L + \pi r L^2}\right) \quad (7)$$

where r and L are the radius and length of the particles, respectively. c equals 1.4 for the cylinders. Introducing $r = 170$ nm and $L = 7$ μm for the sepiolite fibers into eq. (7) yields $\varphi_c =$ 4.7 vol % (10.2 wt %). This result shows that the sepiolite fibers (maximum content 10 wt % in this study) did not form percolated networks in the PLA matrix, which is in agreement with the gradual increase of the measured tensile modulus. As for NCC, its percolation threshold is found to be 29 vol % (10.2 wt %) if the NCC particles are approximated as spheres.[43] Obviously, NCC did not reach percolation in any samples of this study, and thus the modulus of the PLA/NCC composites demonstrated only gradual increase with increasing NCC content.

Dynamic Mechanical Analysis

Figure 8 shows the temperature dependence of G' and tan δ of neat PLA and the various composites. G' plummeted when sample temperature approached the glass transition temperature (T_g ~69°C) of PLA and started to increase at a higher temperature (~90°C) due to the cold crystallization of PLA. Overall, G' of

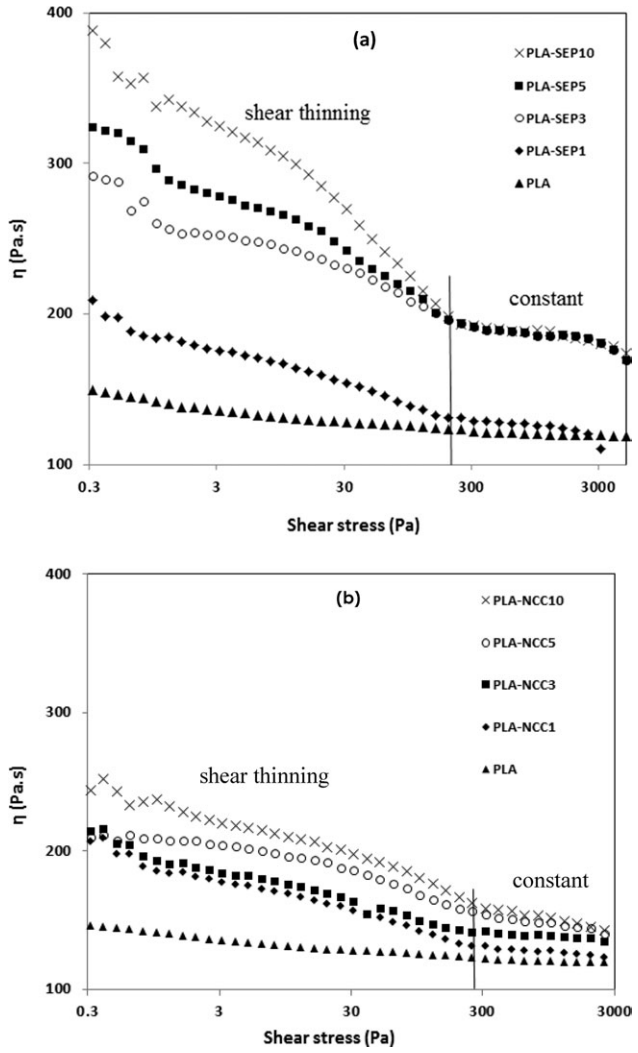

Figure 10. Steady shear viscosity of PLA/SEP (a) and PLA/NCC (b) nanocomposites as a function of shear stress.

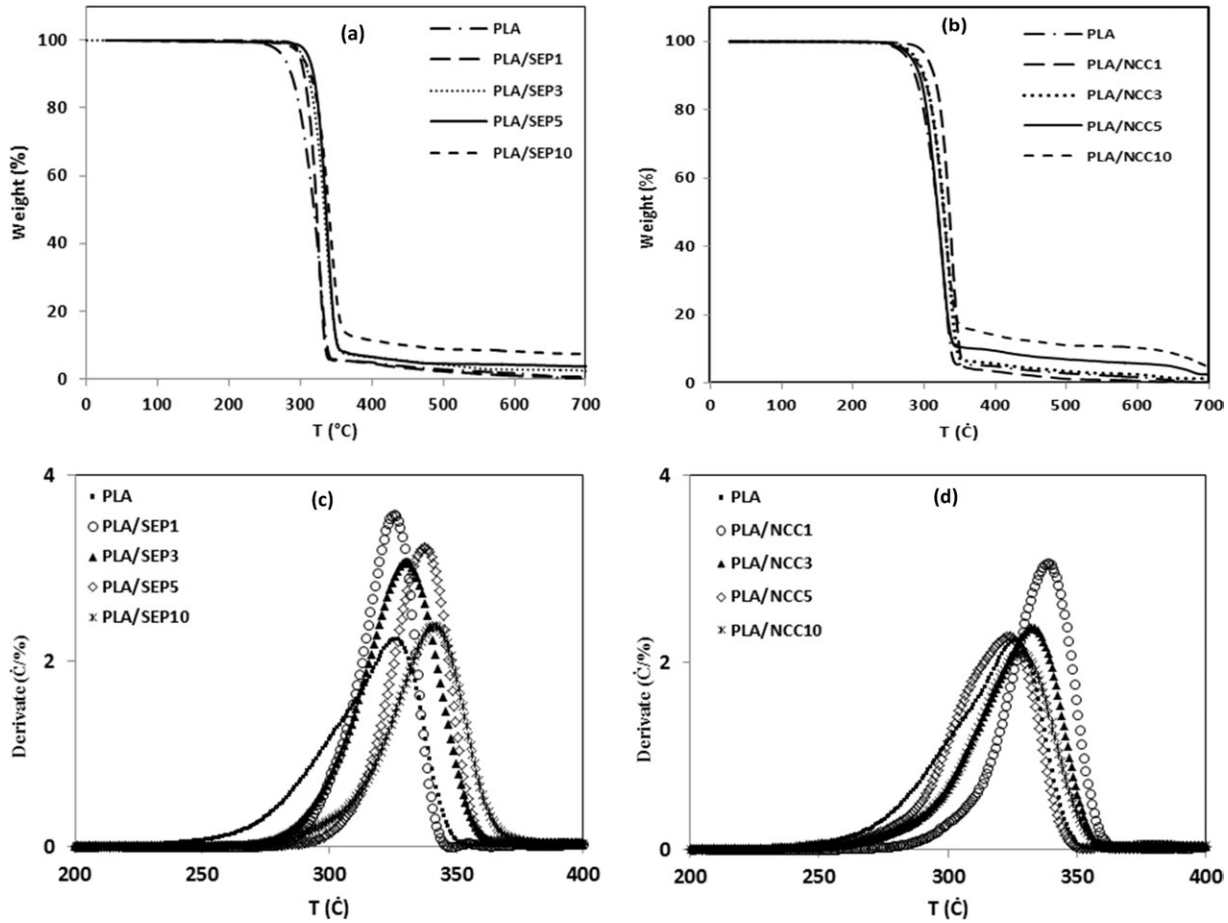

Figure 11. TGA curves for PLA/SEP (a) and PLA/NCC (b) and their corresponding d-TGA curves (c) and (d).

the two nanocomposites increased after the addition of the nanoparticles at both glassy and rubbery states. Tan δ curves showed negligible variation (peak shift and broadening) between the samples, indicating minimal effects of the nanoparticles on PLA chain dynamics during glass transition. It was reported that the plasticizing effect of surfactants could lead to a decrease in T_g of composites.[44] Therefore, the negligible change on the T_g of PLA/NCC can be explained by the two competing factors of the plasticizing effect of NCC surface coating and the restraints on PLA chain mobility exerted by NCC. The minimal change on the T_g of PLA/SEP can be ascribed to their weak interfacial bonding[45] and SEP aggregation.[17] Table II summarizes T_g and G' (measured at 40 and 80°C, respectively) of all the samples.

Melt Rheology

Frequency dependence of G' of the composites comprising different filler loadings are compared in Figure 9. G' increased and the slope of the curves decreased within the low frequency range. The high G' at low frequencies indicated increased elastic behavior of the samples comprising the nanofillers. The decreasing slope indicated that the rheological behavior was increasingly solid-like due to rising filler–filler interactions even the formation of a filler network structure occurred at high filler concentrations.[25] Comparing Figure 9(a) with (b), G' of the PLA/SEP composites increased steadily with SEP concentration, whereas the G' increase of the PLA/NCC was smaller and varied. 1 wt % of NCC led to a remarkable increase in G' of the PLA/NCC, but the increase was smaller at 3 and 5 wt % NCC. The NCC used in this study was coated with fatty acids, which could act as lubricants in the samples. The G' of the PLA/NCC composites was the net result of the G' gain from the filler effects and the G' loss due to the lubrication effect of the fatty acids. Another noteworthy phenomenon was that the critical angular speeds at which the G' of the composites equated to the G' of the neat polymer (indicated by the arrows) were different for PLA/SEP and PLA/NCC. The former showed a higher speed than the later, indicating SEP was able to affected PLA melt flow dynamics to a shorter time scale. This is probably due to SEPs much larger aspect ratio and surface area, which can facilitate the formation of an interconnected filler network (low percolation threshold) and imparted relatively larger confinement on PLA chain mobility.

Steady shear viscosities of the samples were compared in Figure 10. Neat PLA showed a pseudo-Newtonian behavior with nearly constant viscosity. Viscosities of PLA/NCC and PLA/SEP both increased with increasing filler content. Shear thinning of PLA/SEP became increasingly pronounced and was remarkably more significant than that of PLA/NCC. At the same filler

Applied Polymer SCIENCE

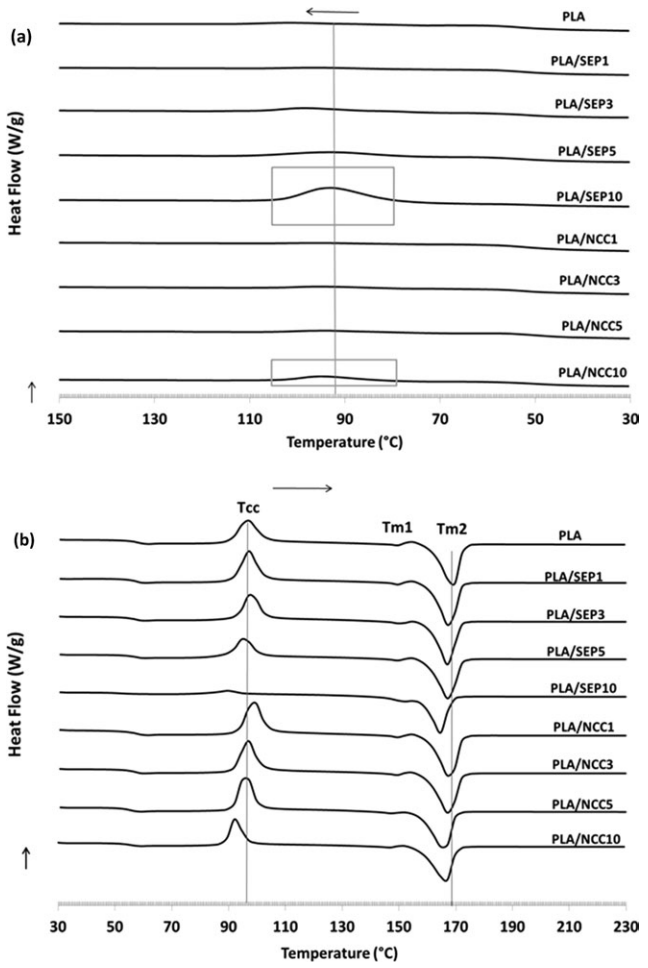

Figure 12. DSC thermograms of neat PLA and its nanocomposites: cooling scan (a) and second heating scan (b). [Color figure can be viewed in the online issue, which is available at wileyonlinelibrary.com.]

content, PLA/SEP exhibited higher viscosities than did PLA/NCC. The shear thinning of filled polymer melts is due to progressive destruction of their original microstructures (filler networks and chain entanglement) and the occurrence of new structures such as filler alignment.

The fact that PLA/SEP exhibited higher viscosity and more pronounced shear thinning than PLA/NCC again indicated that, due to its larger aspect ratio and surface area, SEP formed a more established network structure than did NCC and it imposed stronger restraints on PLA melt flow. A closer observation of each curve of the composites in Figure 10 shows a combination of a shear thinning region at low shear stresses and a relatively constant region at high shear stresses. The two regions were separated using vertical lines in the figures. The transition from the shear thinning region to the constant region indicated that the effects on melt flow from the fillers were largely suppressed by the applied high shear stress.

Thermal Analysis

Thermo Gravimetric Analysis. The weight loss and weight loss rate of the neat PLA and PLA composites are compared in Figure 11. It is clear from Figure 11(c) that T_{max} (the temperature at which the maximum degradation rate occurs) and T_{start} (the temperature at which the sample weight started to decrease) increased with increasing SEP concentration, indicating higher thermal stability. However, the addition of SEP also increased the maximum degradation rate of the composites and the degree of increase appeared to decrease with the SEP concentration. The increase of T_{max} and T_{start} was mainly because that SEP acted as mass transport barrier to the volatiles produced during decomposition and thus delayed the loss of sample weight. Physi- and/or chemi-sorption taking occurring at the matrix-nano particles interphase could also cause to the formation of physical network (especially at high filler content) that could increase thermal stability of composites.[46] It has been reported that SEP can function as a catalyst to accelerate polymer thermal degradation.[47] This could explain the higher weight loss rate after the addition of SEP. The catalyzing effect of SEP was gradually overwhelmed by its barrier property with its increasing concentration. As a result, the weight loss rate decreased.

The effects of NCC on the thermal stability of PLA were much smaller [Figure 11(d)]. Except for 1% concentration, PLA/NCC composites with higher NCC concentrations showed T_{max}, T_{start} and the maximum weight loss rate similar to those of neat PLA. This was believed to be due to NCCs smaller aspect ratio and surface area which resulted in a weaker network structure.

DSC Studies. DSC thermograms for the cooling and the second heating scans of the samples are shown in Figures 12(a) and (b), respectively. Neat PLA showed negligible crystallization during the cooling process. The addition of 5 and 10 wt % SEP and 10 wt % NCC improved of PLA crystallization by acting as nucleation agents. SEP exhibited stronger nucleation effect [larger crystallization peak, Figure 12(a)] because of its larger surface area and higher surface energy compared to surface-coated NCC.

In the second heating scan, the samples showed cold crystallization with T_{cc} (cold crystallization temperature) decreasing with increasing nanoparticle concentration [Figure 12(b)]. The decreasing T_{cc} indicates improved crystallization performance of

Table III. Melting and Crystallization Characteristics of Neat PLA and Its Nanocomposites

Sample	T_{CC} (°C)	$\triangle H_{CC}$ (J/g)	T_{m2} (°C)	$\triangle H_m$ (J/g)	X (%)
PLA	96.0	27.7	169.2	52.8	56.8
PLA/SEP1	97.2	37.9	166.9	51.4	55.3
PLA/SEP3	97.1	34.4	166.5	51.6	55.5
PLA/SEP5	94.7	17.5	165.8	52.1	56.0
PLA/SEP10	86.5	1.6	163.5	56.8	61.0
PLA/NCC1	99.6	27.7	167.3	50.1	53.9
PLA/NCC3	97.0	41.9	167.4	50.9	54.8
PLA/NCC5	94.9	30.5	165.6	52.6	56.6
PLA/NCC10	91.9	41.2	166.5	56.9	61.2

$\triangle H_{CC}$, enthalpy of cold crystallization; $\triangle H_m$, heat of fusion; X, crystallinity (%).
$\triangle H_m$ and X were calculated based on PLA weight.

PLA under the influence of the nanoparticle nucleation agents.[44] At the same nanoparticle concentrations, the samples comprising SEP showed lower T_{cc} compared to those comprising NCC due to SEPs stronger nucleation effect. Melting point (T_{m2}) of the samples decreased with nanoparticle concentration for both composites. This was due to the confinement effect of the nanoparticles, which hindered chain diffusion and folding into crystalline lattice at the crystal growth front. The result was thinner spherulite lamellar thickness and the consequent lower melting points (Table III). Ten et al. found similar effects of cellulose nanowhiskers in polymer nanocomposites.[48] The crystallinity of both composites decreased and then increased with increasing nanoparticle concentration. The crystallinity is controlled by two competing factors, i.e., the nucleation and confinement effects of the nanoparticles. The decrease in crystallinity at low nanoparticle concentrations was due to the dominant influence of nanoparticle confinement. At high concentrations, agglomeration of the nanoparticles led to reduced confinement and thus facilitated crystal growth.[47]

CONCLUSIONS

SEP exhibited much larger aspect ratio and surface area than did NCC. NCC was surface coated with fatty acids to increase its compatibility and resultant dispersion in hydrophobic polymers. This study compared their different effects on the mechanical, dynamic, rheological, and thermal properties of PLA. Both particles increased PLA modulus within the entire concentration range and increased sample strength and failure strain only at low particle concentrations. PLA/NCC showed higher tensile strength and failure strain than PLA/SEP did because of the former's better particle dispersion and stronger interfacial bonding. The two nanocomposites showed similar moduli due to SEPs larger aspect ratio, which compensated for its poor interfacial bonding with the matrix. The larger aspect ratio and surface area of SEP, which facilitated interconnected filler network structure, also led to PLA/SEPs higher storage modulus at low frequency and stronger shear thinning behavior in rheology tests and higher thermal stability in TGA tests. Both nanoparticles functioned as nucleation agents of PLA with SEP showing stronger nucleation effects due to its larger surface area. T_{m2} and crystallinity of the nanocomposites were reduced by both SEP and NCC because their confinement effects hindered crystal growth. At high nanoparticle concentration, the confinement effects decreased because of particle agglomeration, thus leading to increased crystallinity.

REFERENCES

1. Rasal, R. M.; Janorkarand, A. V.; Hirt, D. E. *Prog. Polym. Sci.* **2010**, *35*, 338.
2. Pluta, M.; Paul, M. A.; Alexandreand, M.; Dubois, P. *J. Polym. Sci. Part B: Polym. Phys.* **2006**, *44*, 299.
3. Pluta, M. *J. Polym. Sci. Part B: Polym. Phys.* **2006**, *44*, 3392.
4. Fukushima, K.; Murariu, M.; Caminoand, G.; Dubois, P. *Polym. Degrad. Stab.* **2010**, *95*, 1063.
5. Sinha Ray, S.; Yamada, K.; Okamoto, M.; Fujimoto, Y.; Ogamiand, A.; Ueda, K. *Polymer* **2003**, *44*, 6633.
6. Haand, J. U.; Xanthos, M. *Appl. Clay Sci.* **2010**, *47*, 303.
7. Fukushima, K.; Tabuani, D.; Abbate, C.; Arenaand, M.; Rizzarelli, P. *Eur. Polym. J.* **2010**, *47*, 139.
8. Huang, J. W.; Chang Hung, Y.; Wen, Y. L.; Kangand, C. C.; Yeh, M. Y. *J. Appl. Polym. Sci.* **2009**, *112*, 1688.
9. Jonoobi, M.; Harun, J.; Mathewand, A. P.; Oksman, K. *Compos. Sci. Technol.* **2010**, *70*, 1742.
10. Wangand, B.; Sain, M. *BioResources* **2007**, *2*, 371.
11. Huda, M.; Mohanty, A.; Drzal, L.; Schutand, E.; Misra, M. *J. Mater. Sci.* **2005**, *40*, 4221.
12. Petersson, L.; Kvien, I.; Oksman, K. *Compos. Sci. Technol.* **2007**, *67*, 2535.
13. Zhuang, W.; Liu, J.; Zhang, J. H.; Huand, B. X.; Shen, J. *Polym. Compos.* **2009**, *30*, 1074.
14. Zhao, Y. Q.; Lauand, K. T.; Li, H. L. *Adv. Mater. Res.* **2008**, *47*, 1221.
15. Chrissafis, K.; Paraskevopoulos, K.; Jannakoudakis, A.; Beslikasand, T.; Bikiaris, D. *J. Appl. Polym. Sci.* **2010**, *118*, 2712.
16. Wu, D.; Wu, L.; Zhangand, M.; Zhao, Y. *Polym. Degrad. Stab.* **2008**, *93*, 1577.
17. Murariu, M.; Dechief, A. L.; Bonnaud, L.; Paint, Y.; Gallos, A.; Fontaine, G.; Bourbigotand, S.; Dubois, P. *Polym. Degrad. Stab.* **2010**, *95*, 889.
18. Jiang, L.; Zhangand, J.; Wolcott, M. P. *Polymer* **2007**, *48*, 7632.
19. Jiang, L.; Liuand, B.; Zhang, J. *Ind. Eng. Chem. Res.* **2009**, *48*, 7594.
20. Bilotti, E.; Zhang, R.; Deng, H.; Quero, F.; Fischerand, H.; Peijs, T. *Compos. Sci. Technol.* **2009**, *69*, 2587.
21. Fukushima, K.; Tabuaniand, D.; Camino, G. *Mater. Sci. Eng.: C* **2009**, *29*, 1433.
22. Bilotti, E.; Fischerand, H.; Peijs, T. *J. Appl. Polym. Sci.* **2008**, *107*, 1116.
23. Ma, J.; Bilotti, E.; Peijsand, T.; Darr, J. *Eur. Polym. J.* **2007**, *43*, 4931.
24. Bilotti, E.; Deng, H.; Zhang, R.; Lu, D.; Bras, W.; Fischerand, H. R.; Peijs, T. *Macromol. Mater. Eng.* **2010**, *295*, 37.
25. Vargas, A. F.; Orozco, V. H.; Rault, F.; Giraud, S.; Devauxand, E.; López, B. L. *Compos. Part A: Appl. Sci. Manufact.* **2010**, *41*, 1797.
26. Shen, L.; Lin, Y.; Du, Q.; Zhongand, W.; Yang, Y. *Polymer* **2005**, *46*, 5758.
27. Fukushima, K.; Abbate, C.; Tabuani, D.; Gennariand, M.; Camino, G. *Polym. Degrad. Stab.* **2009**, *94*, 1646.
28. Fukushima, K.; Tabuani, D.; Abbate, C.; Arenaand, M.; Ferreri, L. *Polym. Degrad. Stab.* **2010**, *95*, 2049.
29. Nieddu, E.; Mazzucco, L.; Gentile, P.; Benko, T.; Balbo, V.; Mandrileand, R.; Ciardelli, G. *React. Funct. Polym.* **2009**, *69*, 371.
30. Hapuarachchiand, T. D.; Peijs, T. *Compos. Part A: Appl. Sci. Manufact.* **2010**, *41*, 954.

31. García, N.; Hoyos, M.; Guzmánand, J.; Tiemblo, P. *Polym Degrad. Stab.* **2009**, *94*, 39.
32. Tartaglione, G.; Tabuani, D.; Caminoand, G.; Moisio, M. *Compos. Sci. Technol.* **2008**, *68*, 451.
33. García-López, D.; Fernández, J. F.; Merino, J. C.; Santarénand, J.; Pastor, J. M. *Compos. Sci. Technol.* **2010**, *70*, 1429.
34. Kemal, I.; Whittle, A.; Burford, R.; Vodenitcharovaand, T.; Hoffman, M. *Polymer* **2009**, *50*, 4066.
35. Zhang, L.; Luo, M.; Sun, S.; Maand, J.; Li, C. *J. Macromol. Sci. B* **2010**, *49*, 970.
36. Gu, S. Y.; Zou, C. Y.; Zhouand, K.; Ren, J. *J. Appl. Polym. Sci.* **2009**, *114*, 1648.
37. Available at: http://www.shiraishi-omya.com/C12574D00025C306/vwLookupDownloads/HAKUENKA_CC-R_at.pdf/$FILE/HAKUENKA_CC-R_at.pdf. **2012**. Accessed on October 8, 2012.
38. Agarwal, B. D.; Broutmanand, L. J.; Chandrashekhara, K. *Analysis and Performance of Fiber Composites; Wiley, Hoboken, New Jersey,* **2006**.
39. Chan, C. M.; Wu, J.; Liand, J. X.; Cheung, Y. K. *Polymer* **2002**, *43*, 2981.
40. Du, F.; Scogna, R. C.; Zhou, W.; Brand, S.; Fischerand, J. E.; Winey, K. I. *Macromolecules* **2004**, *37*, 9048.
41. Favier, V.; Chanzyand, H.; Cavaille, J. *Macromolecules* **1995**, *28*, 6365.
42. Balberg, I. *Phys. Rev. B* **1986**, *33*, 3618.
43. Balberg, I.; Anderson, C.; Alexanderand, S.; Wagner, N. *Phys. Rev. B* **1984**, *30*, 3933.
44. Pluta, M.; Jeszkaand, J.; Boiteux, G. *Eur. Polym. J.* **2007**, *43*, 2819.
45. Tingaut, P.; Zimmermannand, T.; Lopez-Suevos, F. *Biomacromolecules* **2009**, *11*, 454.
46. Chivrac, F.; Pollet, E.; Schmutzand, M.; Avérous, L. *Carbohydr. Polym.* **2010**, *80*, 145.
47. Chen, H.; Zheng, M.; Sunand, H.; Jia, Q. *Mater. Sci. Eng. A* **2007**, *445*, 725.
48. Ten, E.; Bahr, D. F.; Li, B.; Jiangand, L.; Wolcott, M. P. *Ind. Eng. Chem. Res.* **2012**, *51*, 2941.